Thermally assisted atom transfer on surfaces

J. W. Gadzuk
Electron Physics Group, National Institute of Standards and Technology, Gaithersburg, Maryland 20899-8412, USA
(Received 5 August 2005; revised manuscript received 22 November 2005; published 1 February 2006)

The low-temperature rates for site-to-site transfer of single atoms and molecules adsorbed on surfaces have been determined in recent scanning tunneling microscopy (STM) studies within the temperature regime where the dominant transfer mechanism changes from mostly activated transmission over to thermally assisted tunneling through the intersite (transition-state) barrier as the temperature is reduced. A model that has provided useful conceptual and quantitative insights into thermally assisted field emission of electrons is used here as the basis for a theory of site-to-site atom transfer in this temperature range where proper account of atomic tunneling and quantum reflection, for energies below and above the transition state barrier, is required. The predicted transfer rates, which are very sensitive to barrier shape as well as height, agree well with those observed in the STM studies of Co and Cu on Cu(111) surfaces in the interesting 4 K$\lesssim T\lesssim$7 K transition range which is relevant in the atom-by-atom fabrication of thermally stable surface nanostructures.

DOI: 10.1103/PhysRevB.73.085401 PACS number(s): 68.43.Jk, 68.43.Pq, 68.37.Ef

I. INTRODUCTION

The scanning tunneling microscope (STM) operated at low temperatures ($\lesssim$20 K) has made possible many stable nearly noise-free experimental studies involving the lateral manipulation of atoms and molecules adsorbed on metallic surfaces.[1–4] Issues related to the microscopic details of site-to-site atom transfer have been of special interest since questions of thermally activated diffusive[5] versus tunneling[6] motion could be meaningfully addressed by observing the temperature dependence of the transfer rate. A fundamental question has been the conditions under which the adsorbate transfer is mainly a result of atom tunneling from site to site as opposed to thermal excitation over an activation barrier separating the "reactant" from the "product," this choice of nomenclature intentionally inviting images of multiple-well potentials from reaction rate theory.[7] In some useful respects, this is reminiscent of a past study on thermal field emission (TFE) spectroscopy which sought to investigate the crossover from pure (electron) tunneling through to thermal activation over the rounded barrier formed by the image potential plus applied field at the surface of a field emission tip.[8,9] Unambiguous interpretation of the spectroscopically observed energy distribution of electrons "transferred" from one side to the other enabled rather definitive conclusions to be made on the details of thermally assisted tunneling that can usefully be applied to the analysis of the nonspectroscopic kinetic atom-transfer studies using the STM. The purpose of the current remarks is to present a model, an extension of the TFE theory, which accounts for the temperature-dependent atom-transfer rate showing the high- and low-temperature limiting forms of Arrhenius and temperature-independent pure tunneling behavior, smoothly and analytically interpolating between these two extremes without having to make either/or specifications. Some of the basic issues and the TFE "solution" are elaborated upon in Sec. II. Connections between thermal tunneling as embodied in TFE,[8] elementary one-dimensional unimolecular reaction rate theory,[7] and the thermal dependence of site-to-site adsorbate transfer observed in recent studies[3,4] are then presented and numerically illustrated in Sec. III. Some concluding thoughts are offered in Sec. IV. Considerations of possible influences of the degrees of freedom associated with additional dimensionality and with other atoms within a polyatomic adsorbate are taken up in the Appendix.

II. THERMALLY ASSISTED FIELD EMISSION

An ensemble of quantum particles initially confined to a spatially localized region by a barrier of finite (energetic) height and (spatial) width will ultimately be found to have some of the particles outside the confining barrier. The in-to-out passage could occur either by quantum tunneling through or thermally assisted transmission "over" the barrier. However, since the hot particles should experience some quantum reflection by the barrier,[10] even when their thermal energy exceeds the barrier height $\equiv\varepsilon_b$, the observable distinction between "tunneling through" and "quantum passage over" may not be so clearcut. The TFE experience illustrates this nicely.

Field emission of electrons occurs when a potential of order 1 keV is applied between the (cathode) tip of a metal wire sharpened to a radius $\sim$50–100 nm and a relatively large anode placed a few centimeters from the tip. The applied voltage produces an electric field $\equiv F$ at the tip whose magnitude is in the range $F\sim$0.1–0.4 V/Å, which when combined with the inherent image potential felt by an electron outside the tip results in an assumed one-dimensional surface barrier

$$V(z) = \phi_e + E_F - e^2/4z - eFz, \tag{1}$$

with respect to an energy zero at the bottom of the conduction band, as shown in Fig. 1. Here ϕ_e is the electron work function and E_F the Fermi energy. The maximum in this barrier is given by $E_m=\phi_e+E_F-(e^3F)^{1/2}=\phi_e+E_F-3.79F^{1/2}$ with F in V/Å, and it is located at a distance $z_m=(e/4F)^{1/2}=1.9/F^{1/2}$ Å from the surface image plane.[11] For the typical

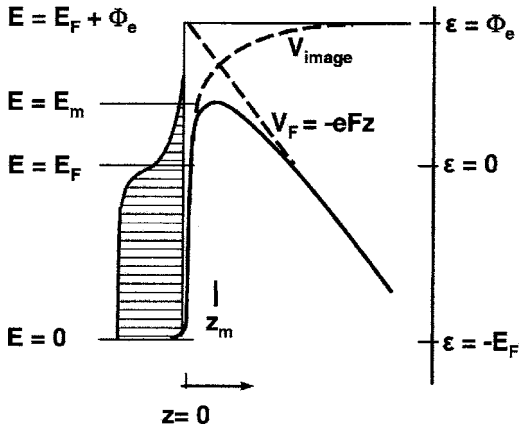

FIG. 1. Model potential at a metal surface under field-emission conditions. The total surface barrier is the sum of the image potential V_{image}, plus that due to the applied field (Ref. 8).

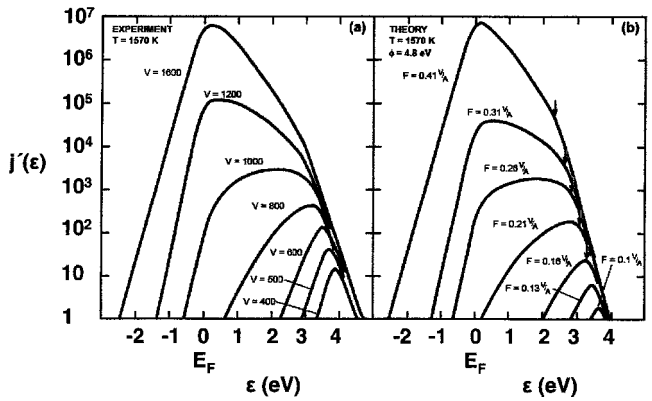

FIG. 2. (a) Experimental TED with emitter-to-anode voltage varied parametrically for $T=1570$ K. (b) Theoretical TED with equivalent field treated parametrically for $\varphi_e=4.8$ eV and $T=1570$ K. The units of j' are arbitrary (Ref. 8).

fields $\sim 0.25\ V/\text{Å}$, $z_m \sim 4$ Å and with $\phi_e \sim 4-5$ eV, the Fermi level barrier thickness is $\lesssim 20$ Å.

The geometry of the field emission spectrometer is such that the total energy distribution (TED) of thermally excited field-emitted electrons is measured. For a three-dimensional free-electron metal, with $\varepsilon = E - E_F$, the TED is given by

$$\frac{dj(\varepsilon)}{d\varepsilon} = j'(\varepsilon) = (4\pi me/h^3) f(\varepsilon) \int_0^{\varepsilon + E_F} D(W) dW, \qquad (2)$$

where $f(\epsilon) = (1 + e^{\epsilon/kT})^{-1}$ is the Fermi function and $D(W)$ is the barrier transmission function which accounts both for tunneling through and passage over the barrier.[9,12] $D(W)$ is integrated over all energetically allowed values of W, the so-called "normal energy" or value of kinetic energy associated with the component of momentum perpendicular to the surface. For tunneling problems it usually suffices to introduce some sort of WKB approximation that leads to a transmission/tunneling probability varying exponentially with barrier height and thickness. This is inadequate when dealing with energies near the barrier top since the transmission must saturate at a value no greater than unity. A venerable WKB-like approximation[13] used by Miller and Good[14] that has proven to be physically reasonable and useful for energies below and above E_m is given by

$$D(W) = [1 + e^{A(W)}]^{-1}, \qquad (3)$$

with the phase integral

$$A(W) \equiv 2 \int_{z_l}^{z_r} \left[\frac{2m}{\hbar^2} (V(z) - W) \right]^{1/2} dz, \qquad (4)$$

in which the classical turning points z_l and z_r are solutions of $V(z) = W$.[14–17] Inserting the surface potential, Eq. (1), into Eq. (4), standard field-emission theory shows that the phase integral can be expressed as

$$A(W) = \frac{4}{3} \left(\frac{2m}{\hbar^2} \right)^{1/2} \frac{(E_F + \phi_e - W)^{3/2}}{eF} v\left(\frac{(e^3 F)^{1/2}}{E_F + \phi_e - W} \right), \qquad (5)$$

where, as discussed by Good and Müller,[18] $v(y)$ is a tabulated elliptic function whose value falls within the range $0 < \nu < 1$, going to zero when $y=0$ and is ~ 0.6 for normal field-emission conditions. The function $\nu(y)$ accounts for the image potential reduction of the pure "triangle barrier" due to the electric field and equals 1 for the triangle barrier without the image potential. Equations (2), (3), and (5) must be numerically integrated to obtain theoretical thermal energy distributions.[19]

A sequence of TFE distributions is shown in Figs. 2(a) (experimental) and 2(b) [theoretical from Eqs. (2), (3), and (5)] with $T=1570$ K, $\phi_e=4.8$ eV, and $E_F \sim 8$ eV. Figure 2(a) displays the measured results obtained using a spherical deflection energy analyzer[9,20] for a series of emitter-to-anode voltages corresponding to electric fields at the tip ranging from ~ 0.08 to 0.4 V/Å. The striking similarity between the experimental results and theoretical expectations based on the Miller-Good barrier transmission function can be seen in Figs. 2(a) and 2(b). There are three distinct energetic regions. The two extrema are characterized by exponentially decaying tails at (i) low energy with a (positive) slope dictated by Eq. (5), the expression which when exponentiated provides the standard field emission tunneling probability, and (ii) high energy with a (negative) slope $=-1/kT$ due to the Boltzman tail of the Fermi function. The intermediate transition region, roughly between the Fermi level and the top of the barrier [marked by arrows in Fig. 2(b)], has either a positive or negative slope depending upon the values of field (or, more generally, the barrier size and shape) and temperature which in turn determine the relative importance of tunneling versus thermal enhancement for a given set of conditions. In all cases there is a distinct change of log slope near the barrier top which is both predicted and observed for this $T=1570$ K example. The dominant contribution to the total current may be mainly due to tunneling ($F \gtrsim 0.3$ V/Å curves), pure thermal Arrhenius-type transmission (F

$\gtrsim 0.2$ V/Å), or a nondistinguishable combination of both ($0.2 \lesssim F \lesssim 0.3$ V/Å). This mix is indeed more subtle than was originally anticipated.[8] Related behavior should occur for atomic motion over and/or through barriers separating metastable adsorption sites on a surface, the realization of which we now turn.

III. ATOM TRANSFER: TUNNELING VS ACTIVATED HOPPING

A number of STM studies have been reported on issues involving controlled manipulation of individual atoms or molecules adsorbed on the Cu(111) surface to form some preselected object such as a surface molecule, quantum corral, or other mesoscopic construction.[1–4] The actual fabrication involves dragging single atoms from site to site on the Cu(111) template using the STM tip as the positioning tool.[21] Thermal stability of the composite structure requires deep local minima in the potential-energy surface topology characterizing the adsorbate-substrate system on an energy scale set by the ambient temperature whereas ease of atom transfer in the actual assembly process favors shallow minima or low intersite barriers. The consequences of these conflicting demands have been nicely demonstrated in STM studies on the temperature dependence of the atom-transfer rate for Cu dimer motion on the Cu(111) surface at temperatures below 21 K where the whole range of thermally assisted atom tunneling and transmission processes (similar to those experienced by electrons in TFE, as documented in Sec. II) come into play. The Cu(111) surface is characterized by two inequivalent three-fold hollow sites with slightly different binding energies called the fcc and hcp sites, depending upon their locations with respect to the second layer atoms. Repp and co-workers have ascertained the hopping rate for Cu dimers in terms of the rate for single-atom transfer while still bound to a stationary partner atom.[3] They assumed that the mobile atom moved within the one-dimensional double-well potential shown in the upper portion of Fig. 3 with well minima located at the three-fold hollow sites of the surface. This two-dimensional $ff \rightarrow fh$ displacement closely resembles that of a one-dimensional ($f \rightarrow h$) hindered rotor centered on the fixed (f) atom. For such transfer in which one atom remains fixed in a fcc site and the other moves between the closest fcc and (slightly less bonded by ~ 1.3 meV) hcp site, the relevant surface crystallography requires that the minima be separated by a distance $d = 1.47$ Å. The main reported observations for present purposes were dimer ff-to-fh hopping rates as a function of temperature in the range $4\ \text{K} \lesssim T \lesssim 7$ K. For $T \gtrsim 6$ K, they represent the thermally activated transfer as process A in Fig. 3, which is analogous to the electron emission responsible for the high-energy leading edge in Fig. 2. As T is reduced to ~ 4 K, the transfer rate becomes more or less independent of temperature which is the widely accepted signature for pure tunneling transfer,[3–7,22] as exhibited in the low-energy experimental cutoff of electron emission in Fig. 2 and depicted as process B in Fig. 3. Similar low-temperature tunneling transfer in the range $2.3\ \text{K} \lesssim T \lesssim 4$ K has been observed by Stroscio and Celotta for single-Co-atom transfer also on the Cu(111) surface.[4] Within the temperature range $4\ \text{K} \lesssim T \lesssim 6$ K, dimer transfer occurs via a thermally activated tunneling process like that which is responsible for the transition behavior in the field electron energy range $0\ \text{eV} < \epsilon \lesssim 3$ eV shown in Fig. 2 and schematically represented as C in Fig. 3.

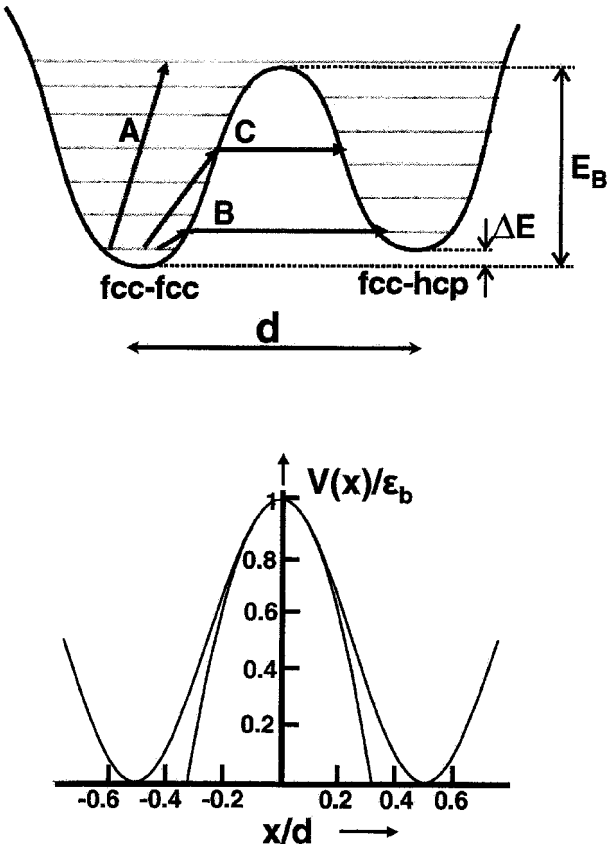

FIG. 3. Top: double-well potential used by Repp *et al.* for atom transport on surfaces via (A) activated hopping, (B) pure tunneling, and (C) thermally assisted tunneling. Bottom: analytic sinusoidal and parabolic intersite barriers used to obtain Eqs. (9) and (10) phase integrals.

The simple unified formulation that accounted well for all the observed features in the TFE studies is now adopted as the basis for a quantitative model of thermally assisted surface atom transfer without need to make any explicit decisions on quantum tunneling versus thermally activated diffusion mechanisms. To this end, the normalized one-dimensionalized transfer rate, in analogy with Eq. (2), is

$$\frac{dn}{dt} = \nu_0 \int_0^\infty D(\epsilon) f(\epsilon) d(\epsilon/kT), \tag{6}$$

where ν_0 is an *appropriate preexponential* with (suggestive but perhaps misleading[7,23]) units of (attempt) frequency, $D(\varepsilon)$ is the barrier transmission function given by Eqs. (3) and (4) evaluated with the relevant atomic mass and potential energy function, and $f(\varepsilon) = e^{-\epsilon/kT}$. An extensive discussion of "beyond one-dimensional modeling" is given in the Appendix. Following Repp *et al.*,[3] a parabolic simplification to

$$V_s(x) = (\varepsilon_b/2)[1 + \cos(2\pi x/d)], \tag{7}$$

their assumed sinusoidal approximation of the double-well potential can be written as

$$V_s(x) \simeq \varepsilon_b - \frac{1}{2}\left(\frac{2\pi^2\epsilon_b}{d^2}\right)x^2, \quad |x| \leq d/\pi;$$
$$= 0, \quad \text{otherwise}, \tag{8}$$

which is sometimes expressed in terms of a characteristic parameter $\omega_b = (\pi/d)(2\epsilon_b/m)^{1/2}$. While ω_b has dimensions of angular frequency, it should really be regarded as a mass-weighted alternative specification of the curvature (thus extension) of the parabolic barrier and not as a true frequency associated with oscillatory motion. In Eqs. (7) and (8), the peak-to-peak amplitude of the sinusoidal potential $\equiv\varepsilon_b$ can be thought of as the classical diffusion barrier height and d as the wavelength characterizing the adsorption site separation. With regards to tunneling, assignment of ε_b, d, and the barrier shape (sinusoidal, parabolic, or something else) completely specifies the effective barrier height and width and hence $A(\epsilon)$, the phase integral given by Eq. (4). Using the parabolic barrier, Eq. (8), in Eq. (4), $A(\epsilon)$ easily reduces to

$$A_{\text{par}}(\epsilon) = 2\pi\frac{\varepsilon_b}{\hbar\omega_b}(1 - \varepsilon/\varepsilon_b) = \left(\frac{2m}{\hbar^2}\varepsilon_b\right)^{1/2}\gamma d, \tag{9}$$

where the first form follows an intriguing historical precedent[24] whereas the second more clearly demonstrates the functional form as the product of a "decay constant" (the square root factor) multiplied by $\gamma d[\gamma \equiv 1 - \varepsilon/\varepsilon_b]$, together providing a measure of the barrier height and thickness as seen by the tunneling particle. For comparison, the phase integral evaluated with Eq. (7), the full sinusoidal potential, is

$$A_{\text{sin}}(\varepsilon) = \frac{4}{\pi}\left(\frac{2m}{\hbar^2}\varepsilon_b\right)^{1/2}\gamma^{1/2}E[\sin^{-1}(\gamma^{1/2}), 1/\gamma]d, \tag{10}$$

where $E[\varphi, m] = \int_0^{\varphi}[1 - m\sin^2\theta]^{1/2}d\theta$ is an elliptic integral of the second kind.[25]

Questions about barrier shapes have significant implications when considering site transfer behavior at the low temperatures characteristic of the over-to-through-barrier transition region. This can be seen by considering the sinusoidal and parabolic potential given by Eqs. (7) and (8) and displayed in the bottom portion of Fig. 3. Clearly the barriers are quite similar at higher energies ($\varepsilon/\varepsilon_b \gtrsim 0.65$), whereas for $\varepsilon/\varepsilon_b \lesssim 0.5$, the full sinusoidal barrier is noticeably thicker. This has a profound influence on the low-energy tunneling behavior. The barrier shape influence follows from the ratio of the phase integrals, Eqs. (9) and (10):

$$R_A(\varepsilon/\varepsilon_b) \equiv A_{\text{sin}}(\varepsilon)/A_{\text{par}}(\varepsilon)$$
$$= \frac{4}{\pi\gamma(\varepsilon)^{1/2}}E[\sin^{-1}(\gamma(\varepsilon)^{1/2}), 1/\gamma(\varepsilon)], \tag{11}$$

which is shown in Fig. 4. The importance of this lower-energy enhancement in A_{sin} is emphasized when calculating the exponentially small tunneling probability.

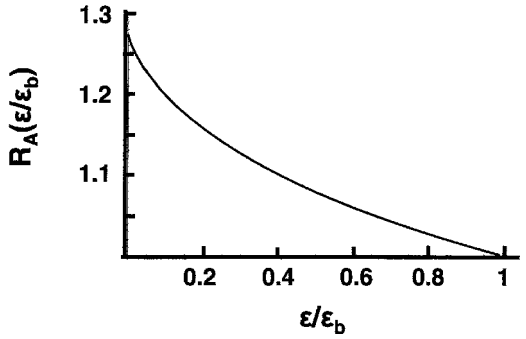

FIG. 4. Ratio of sinusoidal-to-parabolic WKB phase integral as a function of $\xi \equiv \varepsilon/\varepsilon_b$.

It is informative to consider the (nonmeasureable but all-important) one-dimensional energy distribution of the transfer rate implied by Eq. (6),

$$\frac{d\dot{n}}{d(\varepsilon/\varepsilon_b)} = \nu_o(\varepsilon_b/kT)D(\varepsilon)f(\varepsilon), \tag{12}$$

in order to make contact with the TFE considerations outlined in Sec. II. Introducing the dimensionless quantities $a \equiv 2\pi\varepsilon_b/\hbar\omega_b$ and $b \equiv \varepsilon_b/kT$, $(1/\nu_o)(d\dot{n}/d\xi) = bD(\xi;a)f(\xi;b)$ given by Eq. (12) for the parabolic barrier [Eq. (9)] is shown in Fig. 5 as a function of $\xi \equiv \varepsilon/\varepsilon_b$ setting $b=25$, with $a=20$, 25, 30, and 35 appropriate to the low-temperature STM studies of Repp *et al.* These distributions are simpler than the

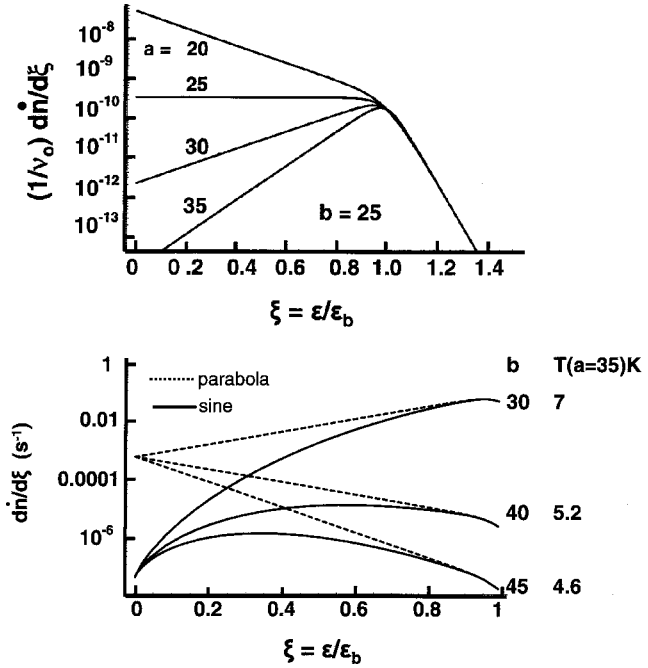

FIG. 5. (a) Energy distribution of the atom-transfer rate over and through a parabolic barrier as a function of $\xi \equiv \varepsilon/\varepsilon_b$ with $b=25$ (or $T=8.35$ K with $\varepsilon_b=18$ meV) and $a=20$, 25, 30, and 35, as labeled. (b) Energy distributions of the atom-transfer rate through parabolic (p) and sinusoidal (s) barriers as a function of $\xi \equiv \varepsilon/\varepsilon_b \leq 1$ with $a=35$ and $b=30$, 40, and 45 (or $T \sim 7$, 5.2, and 4.6 K) as labeled and $\nu_o = 10^{12}$ s^{-1}.

TFE ones which were characterized by three distinct energetic regimes, as discussed in Sec. II. In the present example in which a Maxwell-Boltzmann-distributed flux is incident upon a parabolic barrier, there are only two extended energetic regimes.[26] Pure tunneling occurs for energies between zero and the top of the barrier and quantum transmission for energies above the top. A smooth transition between the two results from the complimentary nature of quantum reflection and transmission and tunneling for energies slightly above and below the barrier maximum[10,17] which is implicitly accounted for in $D(\epsilon)$ given by Eq. (3). Since $D(\epsilon)$ attains an energy-independent maximum value as ϵ rises above the "transition zone" around ϵ_b, the energy dependence of the transfer rate in this limit is simply that of the exponential Maxwellian tail independent of the value of a (which is essentially a measure of the tunnel barrier shape and/or thickness). For the special case of the parabolic or inverted harmonic oscillator barrier[7,24,27], Eq. (9) shows that the WKB phase integral varies linearly with ϵ or ξ. Thus, when combined with the thermal function, the energy distribution in the lower-energy (WKB) range is $d\dot{n}_{\mathrm{WKB}}/d\xi \sim \exp[(a-b)\xi]$, a simple exponential in which the sign of the slope depends on whether the gain from the increased tunneling probability at higher energy exceeds ($a=30,35>b$), precisely equals ($a=25=b$), or fails to match ($a=20<b$) the loss of current due to diminished thermal population of the higher-energy states. For fixed temperature and barrier height and hence fixed b, the a parameter could be varied by changing the barrier curvature ω_b which is equivalent to controlling the barrier thickness. Thicker barriers (unfavorable for tunneling) imply smaller ω_b, hence larger a, which is reflected in the a ordering of low-energy distributions (for a specified choice of ξ) seen in Fig. 5. However, the thinner the barrier, the less of a problem is barrier penetration to begin with and this has the consequence that the gain in barrier transmission does not make up for the loss in numbers of thermally excited atoms (exactly balanced when $a=25=b$). Thus the transfer rate monotonically decreases with increasing energy as typlified by the $a=20$ distribution.

Of considerable relevance is the story behind the similarities and/or differences in calculated energy distributions [Eq. (12)] for the parabolic [Eq. (9)] versus sinusoidal [Eq. (10)] barriers displayed in Fig. 5(b) with $a=35$ and $b=30$, 40, and 45, equivalent to letting $T=7$, 5.2, and 4.6 K. Obviously, for any specified temperature, at a given energy the transfer rate is larger for the parabolic than for the sinusoidal barrier, as already discussed in conjunction with Fig. 4. Also, all parabolic-barrier energy distributions are purely exponential for ξ less than about 0.9 with a slope$=a-b$ whose magnitude and sign are both dependent upon temperature. What is particularly noteworthy is the extreme sensitivity to barrier shape, as exemplified by the contrasting parabolic- and sinusoidal-barrier distributions in the $\sim 4\ \mathrm{K} \lesssim T \lesssim 7$ K range. At the highest temperature, the maximum atom-transfer rate occurs for energies near the top of the barrier independent of barrier shape, as expected for pure thermal activation. More interesting is the intermediate situation around $T \sim 5.2$ K in which maximal passage with a parabolic barrier, occurs for the most populated states, those at the bottom of the barrier, whereas with a sinusoidal barrier, the opposite extreme prevails, maximum transfer rate for the states near the top where the barrier is thinnest in spite of the loss of thermal population. Thus when asked whether it is tunneling or activated hopping, at least at this temperature it is mostly pure tunneling if the barrier is parabolic whereas it is thermally activated tunneling and hopping if the barrier is sinusoidal. Finally, at $T \sim 4.6$ K, the lowest temperature displayed here, the maximum transfer rate involving the sinusoidal barrier occurs with the more populated states which are far below the barrier top, tending towards the pure tunneling limit as T is even further reduced.

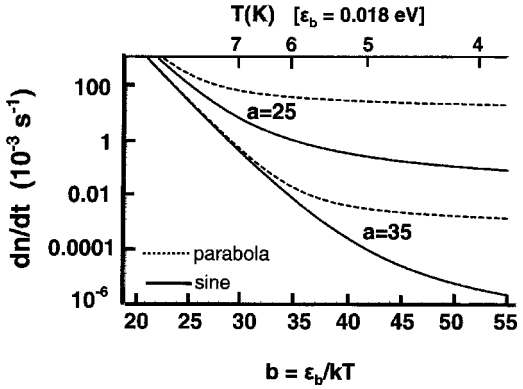

FIG. 6. Total atom transfer rate as a function of $b=\epsilon_b/kT$ for both parabolic and sinusoidal barriers, with $a=25$ and 35, the latter value suggested by Repp *et al.* as appropriate for their Cu-on-Cu(111) data also shown in the figure. The temperature scale is displayed at the top of the figure.

Of course the STM studies do not have the possibility afforded field-emission spectroscopy of measuring the energy distribution of the transferred particles.[9] Therefore the integrated transfer rate [Eq. (6)] is the only experimentally accessible quantity. The theoretical transfer rates that follow from Eqs. (3), (6), (9), and (10) for both the parabolic and sinusoidal barriers are shown in Fig. 6 as a function of $b=\varepsilon_b/kT$ corresponding to temperatures $\sim 4\ \mathrm{K} \lesssim T \lesssim 9$ K when $\varepsilon_b=0.018$ eV. The a parameter has been assigned values of 25 and 35, the latter being deduced from the experiments of Repp *et al.*[3] These curves follow the generic form of high-temperature exponential Arrhenius behavior blending into a temperature-independent low-T limit.[6,22] The details within the transition region shown here are sensitive to both the magnitude of a, the hybrid measure of the barrier height and width, and the barrier shape. In the low-temperature limit, the overall transfer rate for surface atoms confined by the sinusoidal barrier is nearly three orders of magnitude less than for the equivalent parabolic barrier which demonstrates how important knowledge of the intersite potential is if one requires quantitative predictive power for atomic transport rates in the tunneling regime. It should be reemphasized that in spite of barrier-shape issues, the rate does show the venerable T-dependent topological form ubiquitous to thermal studies of this sort.[6,7,22]

Finally the transfer rates calculated from Eqs. (3), (6), (9), and (10) are shown in Fig. 7, now as a function of inverse temperature to facilitate comparison with the observed rates that are also displayed in the figure. Suggested values for the

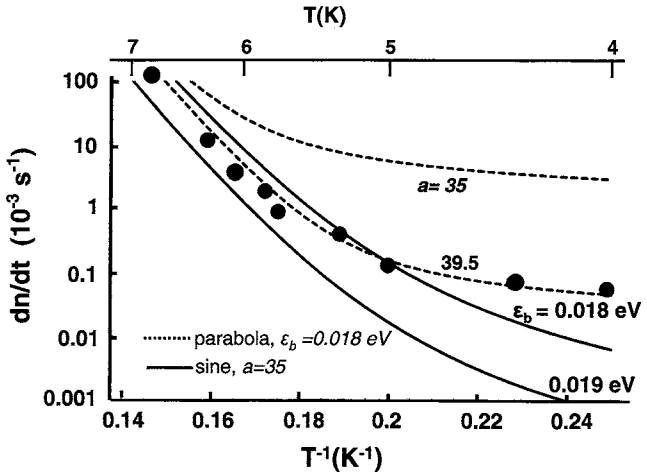

FIG. 7. Total atom-transfer rate as a function of T^{-1} for sinusoidal (solid lines: $a=35$, $\varepsilon_b=0.018$ eV, 0.019 eV) and parabolic (dashed lines: $\varepsilon_b=0.018$ eV, $a=35$, 39.5) using parameters suggested by Repp *et al.* as appropriate for their Cu-on-Cu(111) data also shown in the figure.

input parameters inferred from the data of Repp *et al.* include $\nu_0 \simeq 0.8\times 10^{12}\ \mathrm{s}^{-1}$, $\varepsilon_b \simeq 0.018$ eV, and $d=1.47$ Å, which, with $k_{\mathrm{ads}}=m\omega_b^2=2\pi^2\varepsilon_b/d^2$ [from Eq. (8)] implies that $\hbar\omega_b \simeq 0.003\,28$ eV and thus $a\simeq 35$. The curves in Fig. 7 again convey the sensitivity to both barrier shapes and characteristic parameters, at least in the temperature range of interest here. With the recommended $\varepsilon_b \simeq 0.018$ eV and $a\simeq 35$, the sinusoidal (hence thicker) barrier better reproduces the low-T order of magnitude of the transfer rate than does the parabolic barrier that is obtained from the ($\varepsilon_b \simeq 0.018$ eV, $a \simeq 35$) quadratic form in the expansion of the sinusoid. However, the measured rate of change with temperature below $\sim$5 K looks to more closely follow that of this parabolic barrier. Variation of ε_b shifts (without distorting) the sinusoidal barrier curves as exemplified by the two examples shown in Fig. 7. Thus choice of barrier height does not seem to be the source of the discrepancy between the observed and sinusoidal behaviors. Furthermore, all the rates approach a shape-independent Arrhenius high-temperature limit with a logarithmic slope$=-\varepsilon_b$ which requires that $\varepsilon_b \simeq 0.018$ eV within the experimental error limits. However, if one permits a (or, equivalently, ω_b and/or d) to be varied, then the parabolic barrier characterized by $\varepsilon_b \simeq 0.018$ eV, $a=39.5$ (or $\hbar\omega_s=0.0029$ eV) reasonably reproduces the experimental low-temperature-dependent atom site-to-site transfer rates. The price that has been paid for allowing this "best-fitting" procedure is the sacrifice of the purity of the a parameter, as used up to this point. So far, it has provided a rigorous link between the sinusoidal potential (which allows for the introduction of d, the natural length scale of the double-well problem) and one particular parabolic barrier, that one whose curvature at the barrier top is identical with that of the sinusoidal barrier. In fact, there is no physical reason why this parabolic barrier is any more meaningful than any other one, provided the thickness of the barrier separating the two sites is $<d$, the distance between them. Arguing sinusoid versus parabola is akin to "fitting" a barrier shape (using predetermined "size" parameters) and as such is no more fundamental than choosing a shape (e.g., parabola) and fitting its width (as embodied here in a). In fact, the parabolic barrier that provided the best fit in Fig. 7, that one with $a=39.5$, and hence $\hbar\omega_s=0.0029$ eV, if plotted in Fig. 3, would intercept the x/d axis at 0.362 rather than at 0.32 as shown for the "pure" parabolic offspring of the sinusoid, a distinction that should not alter the qualitative picture. Still it is satisfying to see that reasonable models, even if not definitive, credibly produce site-transfer rates that are in accordance with thoseobserved. Various implications of atom-transfer life beyond one dimension and why they are not likely to be important here are taken up in the Appendix.

IV. SUMMARY

The underlying rate-determining aspect of atomic site-to-site transfer kinetics that is possible for atoms adsorbed on solid surfaces has provided the focus for this theoretical inquiry. Of particular interest has been the characteristics in the low-temperature region where the rate changes from a thermally driven Arrhenius (high-T) to temperature-independent (low-T) behavior. The intermediate transfer regime of interest and relevance in atomic-scale STM manipulations is characterized by thermally assisted tunneling and thermally activated above-barrier hopping (with quantum reflection), both of which must be treated on an equal footing. This has been carried out in the spirit of past work in the area of thermally assisted field electron emission[8,9] in which a modified form of the WKB tunneling probability advanced by Miller and Good[14] has been the essential ingredient enabling smooth transition between the asymptotic Arrhenius and temperature-independent limits. With regards pure tunneling, the sensitivity of intersite tunneling rates to the shape of the barrier has been demonstrated. With the not-unreasonable alternative choices of parabolic versus sinusoidal potentials, for a given barrier height the theoretical low-temperature tunneling transfer rate differs by nearly three orders of magnitude in the case of Cu on Cu(111). Experimentally ascertained transfer rates show "best" agreement with theoretical expectations based on a parabolic intersite barrier slightly thicker than that one which would be inferred from an equivalent sinusoidal potential evaluated with the barrier height and surface lattice spacing parameters determined by Repp and co-workers.[3] Thus one concludes that knowledge of the "correct" intersite barrier shape, not just its height and nominal width, is highly desirable in order to predict low-temperature, tunneling-dominated atom-transfer rates at a truly quantitative level.

ACKNOWLEDGMENTS

Very helpful assistance and/or suggestions from Bob Celotta, Mark Stiles, and Joe Stroscio of the Electron Physics Group is greatfully acknowledged. Thanks also to Jascha Repp for providing the data in a convenient format.

APPENDIX

When asking the question as to what relevant physics might have been omitted in this one-dimensional description

of dimer hopping, an obvious response is that it is the degrees of freedom associated with both the other two dimensions of the moving atom and also with other atoms within a polyatomic adsorbate. Consider the possibility of periodic two-dimensional displacements along the surface, first for single-atom transfer. This is just commonplace surface diffusion[5,28,29] frequently treated within the context of transition-state theory (TST).[7,30] For the low temperatures and energies characterizing the present problem, the additional dimension does not provide any qualitatively new paths for travel between sites (such as greater-than-nearest-neighbor hops[5,31] or Levy walks[32]) but only an increased number of nearest neighbors and thus "jump-equivalent directions available to the adatom."[29] This is simply included as a multiplicative correction of order unity in conventional surface diffusion theory.[5,28,29] With regards to the influence of the atom motion orthogonal to the reaction coordinate, it is a well-established result of TST (Refs. 5, 7, and 30) that for a metastable system consisting of a reaction coordinate nonlinearly coupled to $N-1$ orthogonal vibrational degrees of freedom, ν_o, the *appropriate preexponential* introduced in Eq. (6) should be taken as

$$\nu_o \Rightarrow \nu_{\text{ads}}^{(o)} \frac{\prod_{i=1}^{N-1} \omega_i^{(o)}}{\prod_{i=1}^{N-1} \omega_i^{(b)}}, \tag{A1}$$

where the normal-mode frequencies are evaluated both at the position of the local adsorption minimum (o) and also at the saddle point (b) along the reaction coordinate.[7,30] The frequency $\nu_{\text{ads}}^{(o)}$ is just the vibrational frequency determined by the curvature of the potential-energy curve along the reaction coordinate at the adsorption equilibrium site. From a physical point of view, Eq. (A1) accounts for the effects of the change in the higher-frequency modes as the potential energy associated with the low-energy hindered translation changes by ~ 0.018 eV, the height of the barrier of the double well. Certainly such a small perturbation cannot change the product of the orthogonal higher-energy normal-mode frequencies by anything beyond a multiplicative factor of order 1, so within the framework of TST, the additional freedom provided by two dimensions should not alter the simple picture in a quantitatively significant way. To further quantify two-dimensional rate problems of this type it has proven useful[33] to draw upon analogies with isomerization dynamics[34] in which the temporal evolution is calculated for a classical trajectory or a quantum wave packet propagating over a two-dimensional (2D) potential-energy surface that has been synthesized from a double-well potential (representing the two isomeric forms of the system) nonlinearly coupled to a (usually quadratic) potential representing the other degrees of freedom under consideration. Such inquiries have usually focused on issues of chaos and ergodicity.[34–36] While similar studies carried out for the atom-transfer problem considered here could be equally enlightening, this far exceeds the present scope to the present paper.

Moving beyond classical TST, the reaction probability [given by the integral in Eq. (6) for a 1D system] has been extended to multidimensional systems by Miller within the semiclassical limit of quantum TST.[37,38] He demonstrates that when all N degrees of freedom are separable (i.e., normal modes for multiatom systems), then $D(\epsilon)$ in Eq. (6) can be replaced by

$$P(\varepsilon) \equiv \sum_{\underline{n}} D_{1d}(\varepsilon_{\underline{n}}), \tag{A2}$$

where $D_{1d}(\varepsilon_{\underline{n}}) = [1 + e^{A(\varepsilon_{\underline{n}})}]^{-1}$ is the standard one-dimensional tunneling/transmission probability [Eqs. (3) and (4) with translational energy $\epsilon_{\underline{n}}$] and

$$\varepsilon_{\underline{n}} \equiv \varepsilon - \sum_{i=1}^{N-1} \left(n_i + \frac{1}{2} \right) \hbar\, \omega_i^b, \tag{A3}$$

with the summation notation in Eq. (A2) shorthand for

$$\sum_{\underline{n}} D_{1d}(\varepsilon_{\underline{n}}) = \sum_{n_1=0}^{\infty} \sum_{n_2=0}^{\infty} \cdots \sum_{n_{N-1}=0}^{\infty} D_{1d}(\varepsilon_{\{n_1, n_2, \ldots, n_{N-1}\}}). \tag{A4}$$

Since the second term on the right in Eq. (A3) is the vibrational energy in the $N-1$ modes of the activated complex at the saddle point, $\varepsilon_{\underline{n}}$ is the energy remaining as translational energy along the reaction coordinate. An implication of the Miller theory, as conveyed by Eqs. (A2) and (A4) is that "the cumulative reaction probability is simply the sum over all quantum states of the activated complex of the one-dimensional tunneling probability for each state."[37] A key factor is the extent to which any of these (vibrational) states are occupied since for given total energy ϵ, the translational energy inserted into the phase integral, Eq. (4), is so reduced and the consequent tunneling, and hence the reaction probability via the vibrationally excited-state path, tends towards insignificance at the low total energies and temperatures characteristic of the present study. The zero-point energy included in Eq. (A3), for convenience, can be absorbed as a shift in the origin of the energy scale. With these procedures, even classical models have been successfully utilized provided outcomes in which the energy in a mode falls below its zero-point value are not allowed.[39]

Turn now to the specifics of the dimer transfer. It has already been suggested that the dimer transport reported by Repp *et al.*, at least in the plane of the surface, is basically hindered rotation of one of the Cu atoms between an *ff* and *fh* site adjacent to the partner Cu atom that is fixed at an *ff* site. Since both angular and radial displacements beyond the adjacent *ff* and *fh* sites require an extension of the Cu_2 bond, these displacements must overcome a significantly steeper barrier than that of the transition state of the double-well potential shown in Fig. 3. Thus the double-well rather than an extended sinusoidal potential more appropriate for a single atom seems justified for the hindered rotational potential. Radial stretching and compression of the dimer will also require much more force than the gentle rise and fall of the soft hindered rotation which has the consequence that

$\omega_{\text{radial}} \gg \omega_{\text{ads}}^0$ and thus its role is effectively frozen out at the low temperatures of the present study.

The last concern has to do with possible influences associated with motion normal to the surface. This could be particularly important since the corrugation and hence diffusion barrier felt by an adsorbate would be significantly reduced for those atoms in excited perpendicular vibrational states, those with correspondingly greater mean displacement from the surface. However, the disparity between the transverse hindered rotational frequencies ω_b and that of the perpendicular vibrations provides a low-temperature resolution of the problem. To a reasonable approximation, the curvature at the well minimum (hence frequency) of a well-behaved binding potential (e.g., Morse, Lennard-Jones, etc.) of depth D and atomic-scale range is such that $\omega \sim D^{1/2}$. Therefore the ratio of the perpendicular to transverse frequencies is $\omega_z/\omega_b \approx (\varepsilon_{\text{des}}/\varepsilon_b)^{1/2}$ where ε_{des} is the binding energy of the adsorbate to the surface. For Cu on Cu, $\varepsilon_{\text{des}} \sim 3$ eV has been calculated.[40] Since $\varepsilon_b \simeq 0.018$ eV, the $\hbar\omega_z$ vibrational quantum of the perpendicular mode is not only more than a factor of 10 larger than $\hbar\omega_b$ but also considerably in excess of ε_b. Once again, at the low temperatures of this study excited states and thus perpendicular extension of the adsorbate are almost completely frozen out and therefore are of no consequence in the present realization. However, at higher temperatures, the perpendicular extension effect just discussed could become increasingly important.

[1] D. M. Eigler and E. K. Schweizer, Nature (London) **334**, 524 (1990); J. A. Stroscio and D. M. Eigler, Science **254**, 1319 (1991); P. Avouris, Acc. Chem. Res. **27**, 159 (1994); **28**, 95 (1995); X. Bouju, C. Joachim, and C. Girard, Phys. Rev. B **59**, R7845 (1999); J. K. Gimzewski and C. Joachim, Science **283**, 1683 (1999); W. Ho, J. Chem. Phys. **117**, 11033 (2002).

[2] L. Bartels, G. Meyer, and K.-H. Rieder, Phys. Rev. Lett. **79**, 697 (1997); L. Bartels, G. Meyer, K.-H. Rieder, D. Velic, E. Knoesel, A. Hotzel, M. Wolf, and G. Ertl, *ibid.* **80**, 2004 (1998); S. W. Hla and K.-H. Rieder, Annu. Rev. Phys. Chem. **54**, 307 (2003); S. W. Hla, K. F. Braun, and K.-H. Rieder, Phys. Rev. B **67**, 201402(R) (2003).

[3] J. Repp, G. Meyer, K.-H. Rieder, and P. Hyldgaard, Phys. Rev. Lett. **91**, 206102 (2003).

[4] J. A. Stroscio and R. J. Celotta, Science **306**, 242 (2004).

[5] U. Landman, E. W. Montroll, and M. F. Shlesinger, Phys. Rev. Lett. **38**, 285 (1977); J. C. Tully, G. H. Gilmer, and M. Shugard, J. Chem. Phys. **71**, 1630 (1979); J. D. Doll and A. F. Voter, Annu. Rev. Phys. Chem. **38**, 413 (1987); R. Gomer, Rep. Prog. Phys. **53**, 917 (1990); P. Saalfrank and W. H. Miller, Surf. Sci. **303**, 206 (1994).

[6] *Tunneling*, edited by J. Jortner and B. Pullman (Reidel, Dordrecht, 1986); *Atom Tunneling Phenomena in Physics, Chemistry, and Biology*, edited by T. Miyazaki (Springer, Berlin, 2004).

[7] K. J. Laidler, *Theories of Chemical Reaction Rates* (McGraw-Hill, New York, 1969); P. Hänggi and P. Talken, Rev. Mod. Phys. **62**, 251 (1990).

[8] J. W. Gadzuk and E. W. Plummer, Phys. Rev. B **3**, 2125 (1971).

[9] J. W. Gadzuk and E. W. Plummer, Rev. Mod. Phys. **45**, 487 (1973).

[10] P. H. Cutler and J. J. Gibbons, Phys. Rev. **111**, 394 (1958); N. T. Maitra and E. J. Heller, Phys. Rev. Lett. **78**, 3035 (1999); E. J. Heller, J. Phys. Chem. A **103**, 10433 (1999).

[11] P. J. Jennings and R. O. Jones, Adv. Phys. **37**, 341 (1988).

[12] R. D. Young, Phys. Rev. **113**, 110 (1959); R. D. Young and E. W. Müller, *ibid.* **113**, 115 (1959).

[13] E. C. Kemble, Phys. Rev. **48**, 549 (1935).

[14] S. C. Miller and R. H. Good, Jr., Phys. Rev. **91**, 174 (1953).

[15] E. L. Murphy and R. H. Good, Jr., Phys. Rev. **102**, 1464 (1956); S. G. Christov, Phys. Status Solidi **17**, 11 (1966); H. Neuman, Physica (Amsterdam) **44**, 587 (1969).

[16] C. B. Duke, *Tunneling in Solids* (Academic, New York, 1969).

[17] N. Fröman and P. Fröman, *JWKB Approximation* (North-Holland, Amsterdam, 1965); W. H. Miller, Adv. Chem. Phys. **30**, 77 (1975).

[18] R. H. Good and E. J. Müller, in *Handbuch der Physik*, edited by S. Flügge (Springer, Berlin, 1956), Vol. 21, p. 176.

[19] Strictly speaking, if $A(W)$ is to remain real, W must always be less than V. As discussed by Duke (Ref. 15, p. 35), in order to treat barrier crossings in which W exceeds the barrier height, some alternative procedures have been established in which (i) the use of complex values of z_1 and z_2 for $W > V_{\max}$ is incorporated into the evaluation of $A(W)$ or (ii) a parabolic-barrier formula (introduced here in Sec. III) for $D(W)$ is used in this energy range. See also Fröman and Fröman (Ref. 17, pp. 97–101).

[20] C. E. Kuyatt and E. W. Plummer, Rev. Sci. Instrum. **43**, 108 (1972).

[21] D. E. H. Jones, Nature (London) **374**, 835 (1995); U. Kürpick and T. S. Rahman, Phys. Rev. Lett. **83**, 2765 (1999); S. W. Hla and K.-H. Rieder, Superlattices Microstruct. **31**, 63 (2002); K.-H. Rieder *et al.*, Philos. Trans. R. Soc. London, Ser. A **362**, 1207 (2004).

[22] E. Wigner, Trans. Faraday Soc. **34**, 29 (1938); R. Baer, Y. Zeiri, and R. Kosloff, Phys. Rev. B **54**, R5287 (1996); J. Kuo, L. J. Lauhon, W. Ho, and W. A. Goddard III, J. Chem. Phys. **115**, 5620 (2001); P. G. Sundell and G. Wahnström, Phys. Rev. B **70**, 081403(R) (2004).

[23] G. Iche and Ph. Nozières, J. Phys. (Paris) (Paris) **37**, 1313 (1976).

[24] D. L. Hill and J. A. Wheeler, Phys. Rev. **89**, 1102 (1953).

[25] S. A. Wolfram, *The Mathematica Book*, 4th ed. (Wolfram Media/Cambridge University Press, Champaign/Cambridge, 1999), p. 775.

[26] This is in contrast to the three-regime characteristics seen in TFE associated with the incident flux from Fermi-Dirac-distributed hot electrons. The energetic interval between the Fermi level and the barrier maximum roughly defines the third or transition zone, the feature found in TFE but not thermally assisted atom-transfer energy distributions.

[27] B. C. Garrett and D. G. Truhlar, J. Phys. Chem. **83**, 2921 (1979); R. T. Skodje and D. G. Truhlar, *ibid.* **85**, 624 (1981).

[28] A. F. Voter and J. D. Doll, J. Chem. Phys. **80**, 5832 (1984); S. C. Wang and G. Ehrlich, Phys. Rev. Lett. **68**, 1160 (1992); U.

Kürpick, Phys. Rev. B **64**, 075418 (2001); **66**, 165431 (2002); M.-C. Marinica, C. Barreteau, D. Spanjaard, and M.-C. Desjonquères, *ibid.* **72**, 115402 (2005).

[29] U. Kürpick and T. S. Rahman, Phys. Rev. B **57**, 2482 (1998).

[30] D. G. Truhlar, B. C. Garrett, and S. J. Klippenstein, J. Phys. Chem. **100**, 12771 (1996); G. A. Voth and R. M. Hochstrasser, *ibid.* **100**, 13034 (1996).

[31] K. D. Dobbs and D. J. Doren, J. Chem. Phys. **97**, 3722 (1992).

[32] M. F. Shlesinger, B. J. West, and J. Klafter, Phys. Rev. Lett. **58**, 1100 (1987).

[33] J. W. Gadzuk, J. Opt. Soc. Am. B **4**, 201 (1987); T. S. Jones, S. Holloway, and J. W. Gadzuk, Surf. Sci. **184**, L421 (1987).

[34] N. De Leon and B. J. Berne, J. Chem. Phys. **75**, 3495 (1981); S. K. Gray and S. A. Rice, *ibid.* **86**, 2020 (1987); S. Okuyama and D. W. Oxtoby, *ibid.* **88**, 2405 (1988); G. Gershinsky and B. J. Berne, *ibid.* **110**, 1053 (1999).

[35] E. J. Heller, J. Chem. Phys. **72**, 1337 (1980); R. L. Sundberg and E. J. Heller, *ibid.* **80**, 3680 (1984); P. Brumer, Adv. Chem. Phys. **70**, 365 (1988); W. A. Lin and L. E. Ballentine, Phys. Rev. Lett. **65**, 2927 (1990).

[36] M. C. Gutzwiller, *Chaos in Classical and Quantum Mechanics* (Springer-Verlag, New York, 1990); H. G. Schüster, *Deterministic Chaos: An Introduction*, 3rd ed. (VCH, Weinheim, 1995); J. R. Dorfman, *An Introduction to Chaos in Nonequilibrium Statistical Mechanics* (Cambridge University Press, Cambridge, England, 1999).

[37] W. H. Miller, J. Chem. Phys. **62**, 1899 (1975).

[38] W. H. Miller, Science **233**, 171 (1986); Chem. Rev. (Washington, D.C.) **87**, 19 (1987).

[39] J. M. Bowman, B. Gazdy, and Q. Sun, J. Chem. Phys. **91**, 2859 (1989); W. H. Miller, W. L. Hase, and C. L. Darling, *ibid.* **91**, 2863 (1989); T. D. Sewell, D. L. Thompson, J. D. Gezelter, and W. H. Miller, Chem. Phys. Lett. **193**, 512 (1992).

[40] C. Ghosh, A. Kara, and T. S. Rahman (unpublished).